Effects of Gadolinium on Ion Channels in the Myelinated Axon of *Xenopus laevis*: Four Sites of Action

Fredrik Elinder and Peter Århem
The Nobel Institute for Neurophysiology, Karolinska Institutet, S-171 77 Stockholm, Sweden

ABSTRACT The action of gadolinium (Gd^{3+}) on ion currents in myelinated axons of *Xenopus laevis* was investigated with the voltage clamp technique. The analysis revealed the following effects. (i) The potential-dependent parameters of both Na and K channels were shifted. The shift was equally large for activation, inactivation, and activation time constant curves (+9 mV for 100 μM Gd^{3+}). The effects could be explained by screening of fixed surface charges at a density of −1.2 e nm^{-2}. (ii) The rate of gating for both Na and K channels was reduced more than predicted from the shift. This effect could be quantified as a scaling (by a factor 3 and 5 respectively at 100 μM Gd^{3+}) of the activation time constant curves. (iii) An activation- and inactivation-independent block of both Na and K channels, obeying 1:1 stoichiometry with a K_d value of about 70 μM potential-independent block of leakage current, obeying 1:2 stoichiometry with a K_d value of 600 μM. (iv) The analysis suggests separate binding sites for the effects, comprising high affinity modulatory and blocking sites on the channel proteins and low affinity receptors on phospholipids, associated with the effect on the leakage current.

INTRODUCTION

Several metal ions play fundamental roles in normal cell physiology, in medical treatment, and as toxic agents (Frausto da Silva and Williams, 1991). Most metal ions studied have been reported to shift the potential-dependent parameters of voltage-gated channels along the potential axis. This has been explained in terms of the surface charge hypothesis: the ions modify the electric field across the membrane by screening and/or altering the density of fixed surface charges (Frankenhaeuser and Hodgkin, 1957; Chandler et al., 1965; Gilbert and Ehrenstein, 1969; Brismar, 1973; Hille et al., 1975; Århem, 1980b; for overviews see McLaughlin, 1989; Hille, 1992). However, this explanation has several shortcomings. The most serious is that different ions with the same charge shift gating parameters of the same channel by unequal amounts (e.g., Ni^{2+} and Zn^{2+}; Dodge, 1961; Århem, 1980b; Gilly and Armstrong, 1982a, b). Recently, Armstrong and Cota (1990) have even demonstrated shifts in the opposite direction for Na channel activation and deactivation rate constant curves by the trivalent lanthanum ion (La^{3+}), thereby excluding any explanation by the surface charge hypothesis. In addition to the shift effect, several ions have also been proposed to directly block Na and K channels (e.g., Armstrong and Cota, 1990, 1991; Sheets and Hanck, 1992). The relation between the shift effect and the block is still unclear (Armstrong and Cota, 1991).

To analyze the mechanisms of the metal ion effects mentioned, we chose to study the action of the trivalent gadolinium ion (Gd^{3+}). As a lanthanide, it is closely related to La^{3+}, which has been analyzed extensively (Takata et al., 1966; Vogel, 1974; Århem, 1980a; Brismar, 1980) and has been used, as mentioned above, in the attempts to refute the surface charge hypothesis (Armstrong and Cota, 1990). It is also chemically close to Ca^{2+}, the most abundant divalent ion in living organisms. The close relationship between Gd^{3+} and Ca^{2+} is reflected in size (ionic radius of Gd^{3+} is 1.05–1.11 Å and of Ca^{2+} is 1.00–1.06 Å), bonding, coordination, and donor atom preference (Evans, 1990). Gd^{3+} has been shown to block certain stretch-activated channels and has been used as a selective blocker for identifying these channel types (Yang and Sachs, 1989; Swerup et al., 1991; Zhou et al., 1991). It has also been shown to block voltage-activated Ca and K channels (Docherty, 1988; Lansman, 1990; Swerup et al., 1991). However, no information on its effects on voltage-activated Na channels or on gating of ion channels in general is available.

We have analyzed the effects of Gd^{3+} on currents in voltage-clamped axons from *Xenopus laevis*. All ion currents, including the leakage current (I_L), were found to be dose-dependently affected, but each in a different manner. The different effects suggest different mechanisms. In particular, we have analyzed the results with reference to the surface charge hypothesis and found that they were compatible with such a hypothesis. Essential for this conclusion was the finding that the Gd^{3+} effect on the voltage dependence of the time constants could be separated into a shift and a scaling effect. This separation made it possible to resolve several seemingly conflicting results in the literature, including those of Armstrong and Cota (1990).

In a following paper (Elinder and Århem, 1994), we will develop a model for the Gd^{3+} effects on the gating and the change in membrane electric field. Some of the results have been presented elsewhere (Elinder and Århem, 1991b).

Received for publication 16 August 1993 and in final form 22 April 1994.

Address reprint requests to Peter Århem, The Nobel Institute for Neurophysiology, Karolinska Institutet, S-171 77 Stockholm, Sweden. Tel.: 46-8-728-64-03; Fax: 46-8-34-95-44.

0006-3495/94/07/71/13 $2.00

MATERIALS AND METHODS

Voltage-clamp method

Large myelinated fibers were isolated from the sciatic nerve of unanesthetized decapitated toads of the species *Xenopus laevis*. Single fibers were

mounted in a recording chamber and cut at half-internode length on both sides of the node under investigation. Vaseline seals were used to separate the electrolyte solutions. The chamber was connected by KCl bridges to the voltage-clamp apparatus. The chamber design, circuitry, and balancing procedures were essentially the same as described by Dodge and Frankenhaeuser (1958), with the modifications described by Århem et al. (1973). To obtain good feedback control and recording situations, all experiments were performed at a relatively low temperature (8–10°C).

Data acquisition

Pulse generation and sampling were made using a TL-1 DMA interface (Labmaster, Axon Instruments, Foster City, CA) and the pCLAMP software (Axon Instruments). Sampling interval was 10–200 μs.

Solutions

The test solution was applied to the pool with the node and consisted of $GdCl_3 6H_2O$ added to control Ringer solution. The concentration of Gd^{3+} obtained depends on the degree of hydrolysis. Like other lanthanides, Gd^{3+} is known to form different hydroxy and oxo species, which may ultimately polymerize and precipitate. (For an extensive study of the hydrolysis of La^{3+}, see Biedermann and Ciavatta, 1961.) However, at the concentrations and pH used in the present investigation, stable aqueous solutions are formed (see Table 2–10 in Evans, 1990; the upper limit at a Gd^{3+} concentration of 0.01 M is pH 7.57). Using the association constants given by Smith and Martell (1976), the calculated reduction of Gd^{3+} concentration caused by formation of hydroxides (mainly $GdOH^{2+}$) is approximately 4% (at 0.3 M ionic strength and 25°C). This estimation agreed well with the results from a comparison between the effects of test solutions used less than 1 min after preparation and of test solutions used more than 5 h after preparation. No systematic difference in effect was found. The reduction in Gd^{3+} concentration caused by hydrolysis, therefore, was assumed to be relatively small. Precautions were further taken to avoid oxidizing the Gd salt by keeping the batch in a nitrogen-filled container. The Ringer solution contained (in mM): NaCl 115.5, KCl 2.5, $CaCl_2$ 2.0, and Tris buffer (adjusted to pH 7.2) 5.0. The solution applied to the end pools consisted of (in mM): KCl 120.0 and Tris buffer (pH 7.2) 5.0.

Data analysis

Because only relative current values were essential in the present investigation and because the nodal area and axoplasmic resistance were not measured in the experiments, no attempt was made to calibrate the current in absolute values (see Dodge and Frankenhaeuser, 1959). However, to get a quantitative value of the leakage conductance (g_L), we assumed a nodal area of 100 μm^2 and an internodal axoplasmic resistance of 40 MΩ.

The separation of Na and K currents (I_{Na} and I_K) was performed without specific channel blockers, to facilitate a comparison between effects on both Na and K channels of the same fiber. The measured parameters were chosen to avoid interference between the currents. The measured parameters of I_{Na} were peak I_{Na}, time to half peak I_{Na} ($t_{1/2}$) and the time constant of the first exponential falling phase of the inactivation (τ_{inact}) at low potential steps. In no case did the much slower I_K interfere with these measurements. The measured parameters of I_K were steady-state I_K (at 20–100 ms) and time to half-steady-state I_K ($t_{1/2}$). Calculations based on the empirical description by Frankenhaeuser and Huxley (1964) showed that I_{Na} did not interfere with these measurements. The investigation to be presented shows that the interference problem of the measured parameters was even smaller for a fiber in Gd^{3+} solution than for the control case.

The Na permeability (P_{Na}) was calculated from the Goldman-Hodgkin-Katz equation

$$P_{Na} = I_{Na} \frac{RT}{UF^2} \frac{(1 - \exp(-FU/(RT))}{[Na]_i - [Na]_o \exp(-FU/(RT))}, \quad (1)$$

where I_{Na} is the current, $[Na]_i$ and $[Na]_o$ are inner and outer concentrations of Na^+, U is absolute potential, and R, T, and F have their usual meanings (Goldman, 1943; Hodgkin and Katz, 1949; see also Dodge and Frankenhaeuser, 1959). The potassium permeability (P_K) was calculated correspondingly (Frankenhaeuser, 1962).

Activation (normalized P_{Na} vs. potential) or inactivation (steady-state Na inactivation) curves were fitted to a simple Boltzmann distribution:

$$P_{Na} = 1/(1 + \exp((U_{1/2} - U)/k)), \quad (2)$$

where $U_{1/2}$ is the potential at the midpoint value ($P_{Na} = 1/2$), U is the test-step or prepulse potential, and k is the slope value. Normalized P_K was fitted correspondingly.

The analysis of the effects on fixed surface charges (Gouy-Chapman theory) was based on the Grahame equation (modification of Eq. 40 in Grahame, 1947):

$$\sigma^2 = 2\epsilon_r \epsilon_0 RT \sum_i c_i(\exp(-z_i \psi_0 F/(RT)) - 1), \quad (3)$$

where ψ_0 is surface potential, σ is the density of surface charges, c_i is the bulk concentration, and z_i is the valence of ith ionic species. ϵ_r and ϵ_0 are the dielectric constant of the medium and the permittivity of free space and have the values 78 and $8.85 \cdot 10^{-12}$ Fm^{-1} respectively. T, R, and F have their usual meanings.

The dose-response curves were fitted by a least-square method to the equation describing a reversible reaction:

$$I = 1/(1 + (c/K_d)^{KH}), \quad (4)$$

TABLE 1 Effects of Gd^{3+} on I_{Na}, I_K and I_L

Axon	K_d(Na) (μM)	K_H	K_d(K) (μM)	K_H	K_d(L) (μM)	K_H	g_L (mS cm^{-2})	U_L* (mV)
1	50		130		1200			−100
2	100		100					
3	40	0.98	60	0.74	280	0.50		−70
4			100		420		30	−95
5	100	1.15	40	1.14	1200	0.46	35	−75
6			32					
7	80	0.93	180	0.97	420	0.36	45	−55
G‡	69	1.02	78	0.94	590	0.44	36	
x§	74	1.02	92	0.95	700	0.44	37	−79
±SD	28	0.12	47	0.20	460	0.07	8	18

* Crossing-over-potential for I_L as described in Results.
‡ Geometric mean.
§ Arithmetic mean (±SD).

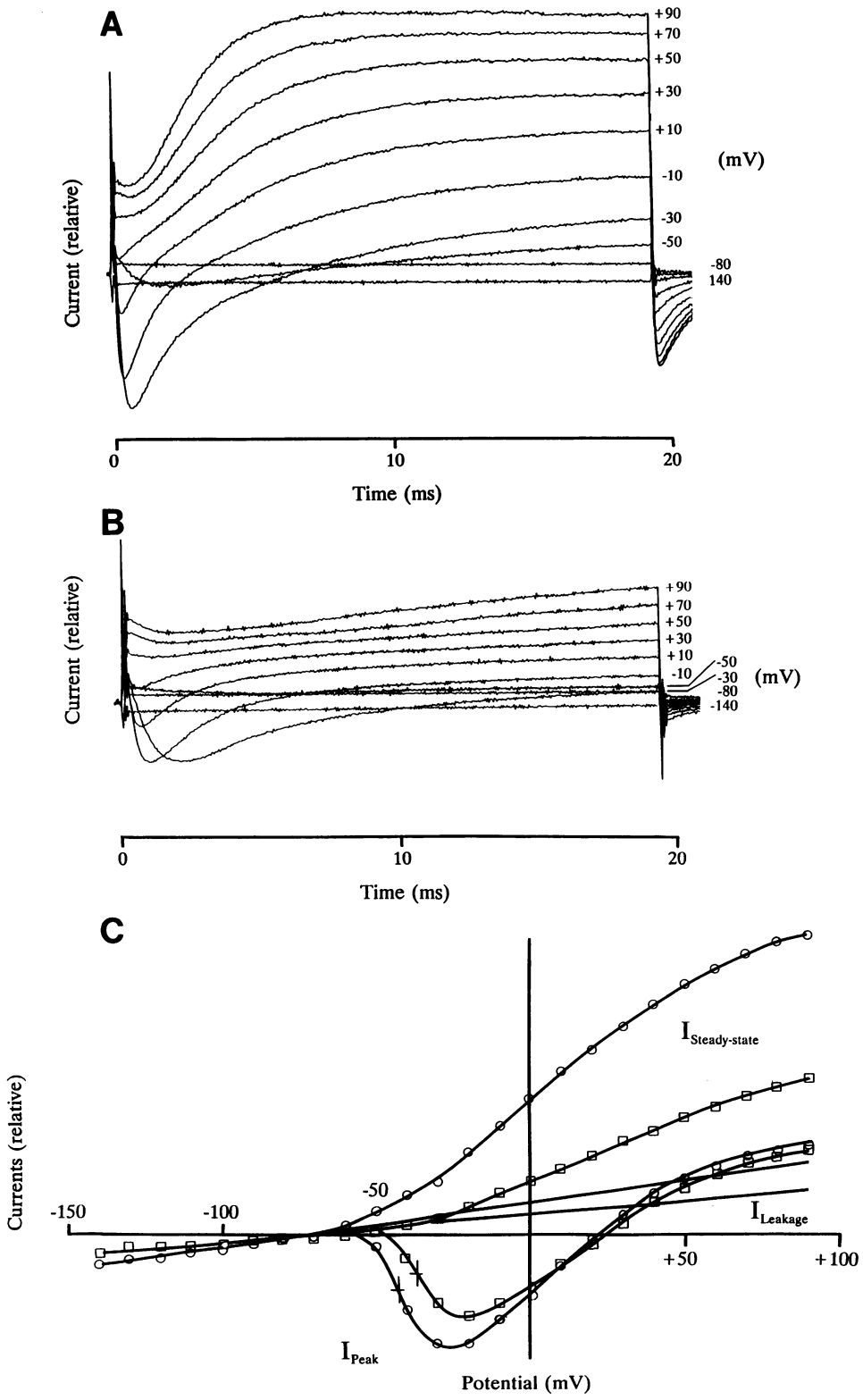

FIGURE 1 Effects of Gd^{3+} on currents associated with rectangular potential steps as indicated. (*A*) Control solution. (*B*) 60 μM Gd^{3+}. (*C*) Current versus potential relation for control (○) and 60 μM Gd^{3+} (□) solutions. Steady-state current measured after 100 ms. U_H = −110 mV in *A* and *B*, −90 in *C*.

where I is the normalized current, c is the concentration of Gd^{3+}, K_d is the concentration at 50% reduction, and K_H is the Hill coefficient. Because geometric means of K_d and K_H seem more adequate than arithmetic means in the present context (the distribution was less skewed when the values were logarithmized), they were consequently used in the text. In addition, arithmetic means and SDs are given in Table 1. For the quantitative analysis to be presented, we chose to base it on seven consecutive experiments (axons presented in Table 1).

RESULTS

Effects on all of the ion currents were observed at Gd^{3+} concentrations from 10 μM and upwards. Fig. 1 shows typical effects of 60 μM Gd^{3+} on a family of currents associated with rectangular pulse steps. From Fig. 1 *C*, it is seen (i) that I_L was reduced, (ii) that peak I_{Na} was reduced and its potential

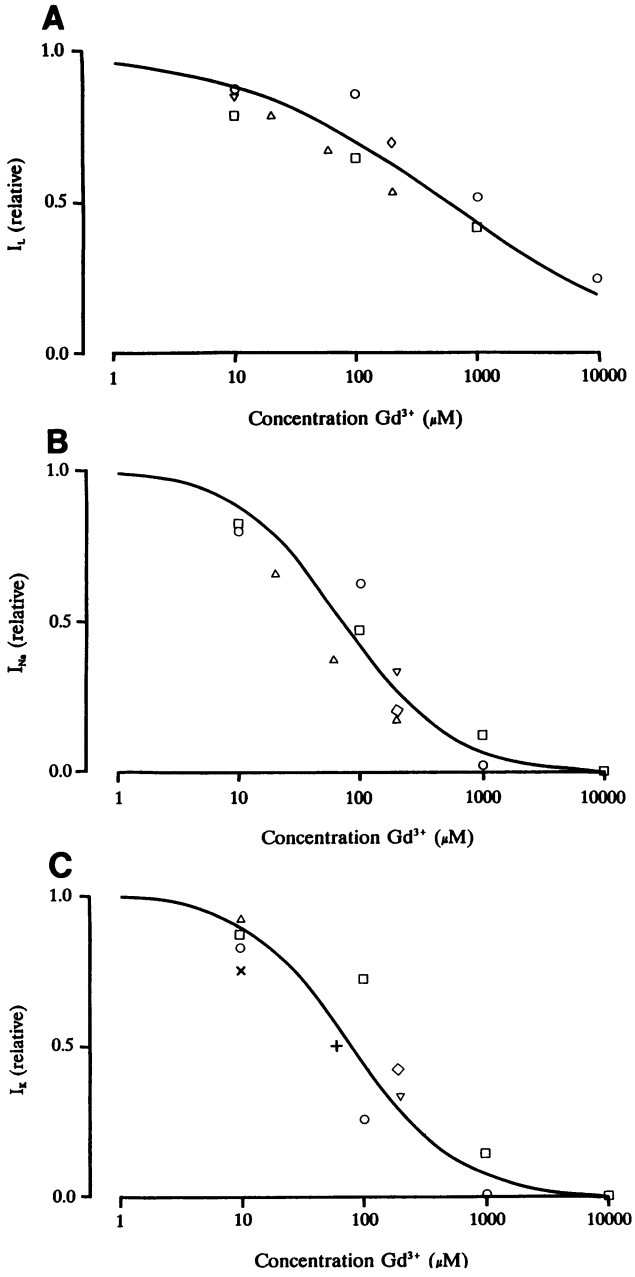

FIGURE 2 Dose-response curves for potential independent effects. Data from seven fibers as indicated by symbols. Continuous lines solutions to Eq. 4. (*A*) Effects on I_L. $U_H = -110$ mV, $K_d = 590$ μM and $K_H = 0.5$. (*B*) Effects on maximum peak I_{Na} at steps to −10 mV. $U_H = -140$ mV, $K_d = 69$ μM and $K_H = 1$. (*C*) Effects on steady-state I_K at steps to +50 mV. $U_H = -90$ mV, $K_d = 78$ μM and $K_H = 1$.

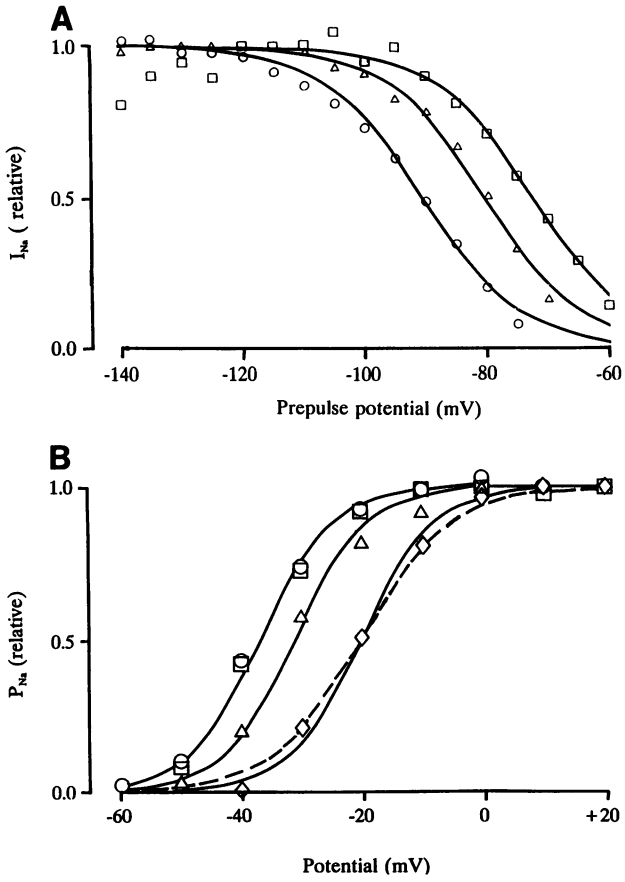

FIGURE 3 Shift of steady-state Na inactivation and Na activation curves. Continuous and interrupted lines solutions to Eq. 2 for various *k*. (*A*) Steady-state inactivation curves at steps to −10 mV for control (○), 60 μM (△), and 200 μM Gd^{3+} (□) solutions. $U_{1/2} = -90$, −80, −72 mV. $k = -8.0$ mV in all cases. (*B*) Peak permeability versus potential curves for control (○), 20 μM (□), 60 μM (▲), and 200 μM Gd^{3+} (◇) solutions. $U_H = -90$ mV. $U_{1/2} = -37$, −31, and −21 mV. $k = 6.0$ mV (——) and $k = 7.5$ mV (- - - -). Same fiber as in *A*.

dependence shifted in the positive direction along the potential axis, and (iii) that steady-state I_K (measured at 100 ms) was reduced and its potential dependence shifted in the positive direction. Further, it is seen (iv) that the reversal potential of peak I_{Na} (U_{rev}) was shifted in the negative direction. From Fig. 1 *C*, it is also clear that the time course of both I_{Na} and I_K was slowed down. The effects were slowly and only partially reversible within the recovery time used, which was less than 5 min to be able to perform reasonably many solution changes per fiber. Furthermore, the reversibility differed from parameter to parameter. The effect on potential-dependent parameters showed a faster and more complete reversibility after 5 min than the effect on other parameters. For simplicity, we assume full reversibility in the calculations below.

Effect on leakage current

The reduction of I_L was measured for currents associated with negative or small positive potential steps. To avoid complications by effects on I_K, the measurements were performed at $U_H = -110$ mV. At this potential, 98% of the slowly activating, noninactivating K channels are reported to be closed (Dubois, 1981). g_L was 36 mS cm^{-2} ($n = 3$; Table 1), in good agreement with previous results on the same preparation (30.3 mS cm^{-2}; Frankenhaeuser and Huxley, 1964). The potential at which control I_L and Gd^{3+} affected I_L curves crossed each other was −79 mV ($n = 5$; Table 1). This is close to previous measurements of the resting potential in

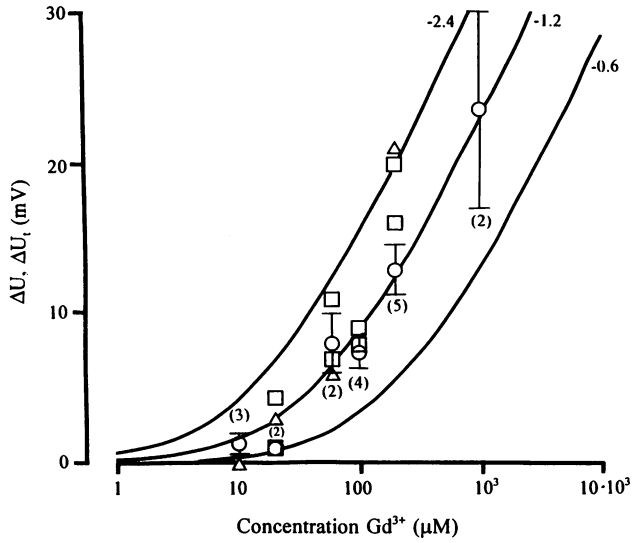

FIGURE 4 Relation between shift of potential-dependent parameters and concentration of Gd^{3+}. Data from five fibers. Shifts of steady-state inactivation and activation curves for the Na-system (mean ± SEM) indicated by (○). Highest and lowest values for ΔU_t from I_{Na} activation (data from two fibers) indicated by (□). ΔU_t from I_K activation (data from two fibers) indicated by (▲). Continuous lines are solutions to Eq. 3 for Gd^{3+} in Ringer solution (for composition see Methods) with surface charge densities as indicated in e nm^{-2}.

myelinated axons (−71 mV; Huxley and Stämpfli, 1951). Fig. 2*A* shows the dose response curve constructed from data of five fibers. K_d was 590 μM (n = 5; Table 1). K_H was 0.44 (n = 3; Table I), suggesting 1:2 stoichiometry.

Effect on Na current

Shift of inactivation and activation curves

As concluded from Fig. 1, the Gd^{3+} effect on I_{Na} was complex. The induced reduction of I_{Na} could, in principle, be caused by modification of the inactivation or activation system or to an inactivation- and activation-independent block. That effects on the inactivation system were involved can be seen in Fig. 3*A*, where the induced shift of 60 and 200 μM Gd^{3+} on the inactivation curve is shown. The inactivation curves were constructed from measurements of the peak I_{Na} at a step to −10 mV from 1-s prepulses of varying potentials (U_{PP}).

Note also in Fig. 3*A* the reduction of the inactivation curve at the most negative potentials for 200 μM Gd^{3+}. This effect was only seen at potentials below −120 mV and, consequently, could not be caused by the approximately +12 mV shift of the inactivation curve, because no reduction was observed for the control curve at potentials down to −140 mV. Such an effect has also been observed for high concentrations of Ca^{2+} and La^{3+} by several authors (Dubois and Bergman, 1971; Vogel, 1974; Rack and Drews, 1989), demonstrating the close chemical relationship between these ions and Gd^{3+}.

The Gd^{3+} effect on the activation system was more difficult to quantify because of the complication of the permeability curve caused by the U_{rev} shift (see Fig. 1 *C*). Fig. 3 *B* shows the normalized permeability values at potential steps up to +20 mV, calculated from Eq. 1. Up to this potential level, the U_{rev} shift of the magnitude seen in the present experiments was estimated to cause negligible effects on the permeability curve. As seen from Fig. 3 *B*, the effect was a concentration-dependent shift along the potential axis. In addition, a slight decrease (about 20%) of slope at the highest concentration (200 μM) was systematically noted, in accordance with reported effects of a number of divalent ions and of La^{3+} (Brismar, 1980; Armstrong and Cota, 1990; Hanck and Sheets, 1992).

Fig. 4 shows the collected shift-values from five fibers for the inactivation and activation curves at different Gd^{3+} concentrations. The ΔU values for both activation and inactivation were found to be about equal and, therefore, were lumped together in the figure (with bars; mean ± SEM). As seen, they are well described by Eq. 3 for a density of −1.2 e nm^{-2} (e is elementary charge).

Inactivation- and activation-independent block

To obtain a dose-response curve for the inactivation- and activation-independent block of I_{Na}, we measured the effect on the peak I_{Na} at steps to −10 mV from a 1-s prepulse of −120 mV. The step value of −10 mV was chosen to avoid complications caused by the shift of the activation curve and the shift of U_{rev}, and the prepulse value of −120 mV was chosen to avoid complications caused by inactivation effects. Fig. 2 *B* shows a dose-response curve constructed from such measurements on five fibers. K_d was 69 μM (n = 5; Table 1). K_H was 1.02 (n = 3; Table 1), suggesting 1:1 stoichiometry.

Effect on time course

Fig. 5 *A* shows the effect of Gd^{3+} on the time course of I_{Na} associated with a potential step from −110 to −10 mV. Both activation and inactivation time courses were clearly slowed down in a concentration-dependent manner. A consequent increase in time-to-peak is also evident: from about 0.4 ms in control solution to about 2 ms in 200 μM Gd^{3+}. The effect could not be explained by the shift of voltage dependence, described above for both activation and inactivation system. This is seen in Fig. 5 *B*, where I_{Na} at a potential step to −20 mV in control solution is compared with I_{Na} in 60 μM Gd^{3+} at a step to −10 mV, corresponding to the shift of the activation and inactivation curves (+9 mV in this fiber). The concentration dependence of the effect on activation and inactivation time courses is shown in Fig. 6. Fig. 6 *A* depicts the effect on the relation between $t_{1/2}$ and potential for different Gd^{3+} concentrations. In contrast to the effect on activation and inactivation curves, the effect on the time constant curves could not be described as simple shifts of potential dependence. However, it could successfully be described by a combination of a shift and multiplication by a scaling factor, as shown by crosses (+). The shift (ΔU_t) and scaling values (A) used to construct the curves in the figure

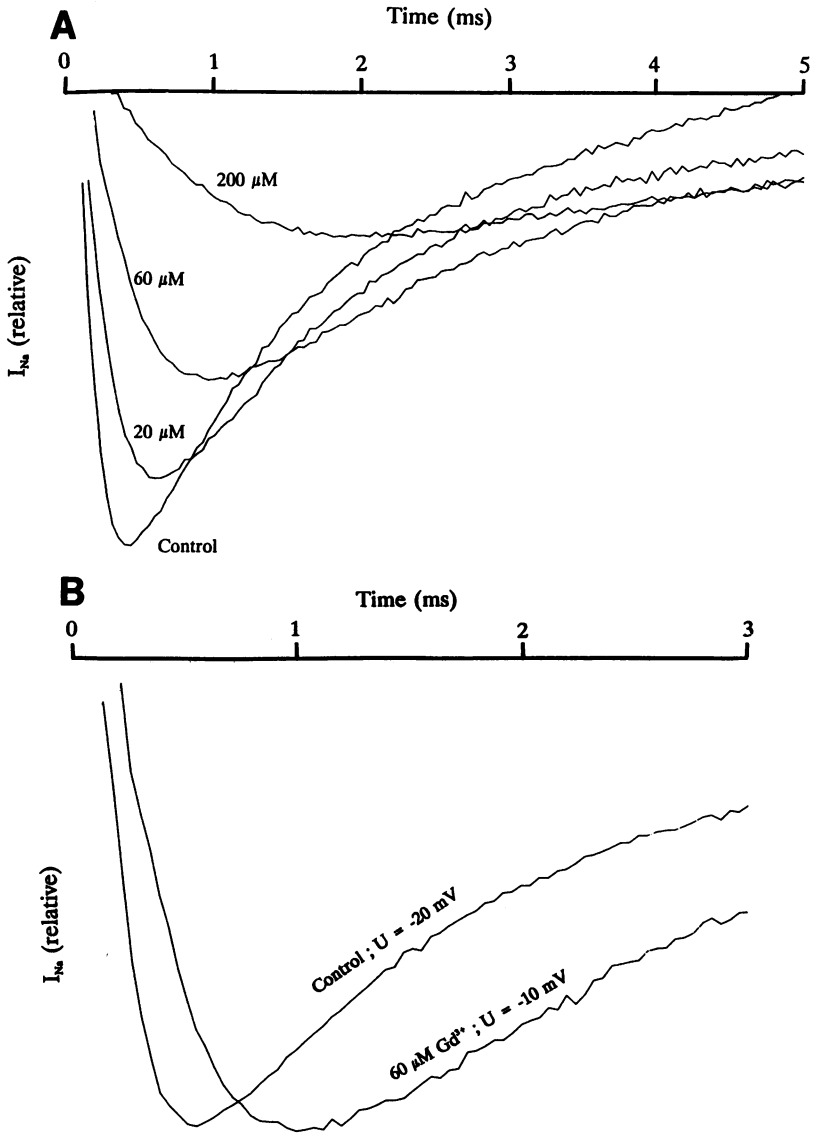

FIGURE 5 Effect on time course of I_{Na}. (*A*) I_{Na} associated with a potential step to −10 mV for different concentrations of Gd^{3+}. $U_H = -110$ mV. (*B*) Normalized I_{Na} in control and 60 μM Gd^{3+} solution for potential steps as indicated. Same fiber as in *A*.

were obtained by a manual fitting procedure indicated in Fig. 6 *B*. The interrupted lines show the calculated curves for different $\Delta U_t/A$ pairs at 200 μM Gd^{3+}. The best fit was obtained when ΔU_t was in the range 16–20 mV and A was in the range 2.5–2.8. By applying this procedure, we obtained $\Delta U_t/A$ pairs at each concentration. ΔU_t values from such optimal $\Delta U_t/A$ pairs in Fig. 6 *A* are shown in Fig. 4 (*open squares*). As seen, they are well described by Eq. 3 for a charge density of −1.2 e nm^{-2}. The A values for different concentrations from Fig. 6 *A* are shown in Fig. 6 *C* (*open squares*).

Fig. 7 *A* shows the effect on the inactivation time constant curve at different Gd^{3+} concentrations. As for the activation system, these effects could be described as a combined shift and scaling of the curves. The magnitude of ΔU_t, however, was considerably larger, and that of A was considerably smaller than the corresponding values for the activation system; in some cases the effect could be described as a pure shift. Thus, these values seem difficult to reconcile with those of the activation system within a surface charge hypothesis. However, this problem might only be apparent and will be treated in the Discussion.

Shift of reversal potential

The induced negative shift of reversal potential (U_{rev}; see Fig. 1 *C* was systematic and reversible. This is seen in Fig 8 *A*, which shows the reversal potential at increasing Gd^{3+} concentrations in one experiment. The reversibility suggests that the effect was not caused by increased axoplasmic Na^+ concentration. The estimation of the reversal potential was based on the assumption of a voltage-independent g_L. Such an assumption has been questioned for the squid giant axon (Adelman and Taylor, 1961). However, it seems reasonable as an approximation for the myelinated axon. The zero-current (at U_{rev}) in control solution was systematically and reversibly transformed into a transient outward current when the Gd^{3+} solution was applied. The concentration dependence of the shift is shown in Fig. 8 *B*. The mechanism of this effect was not analyzed further here. One explanation is

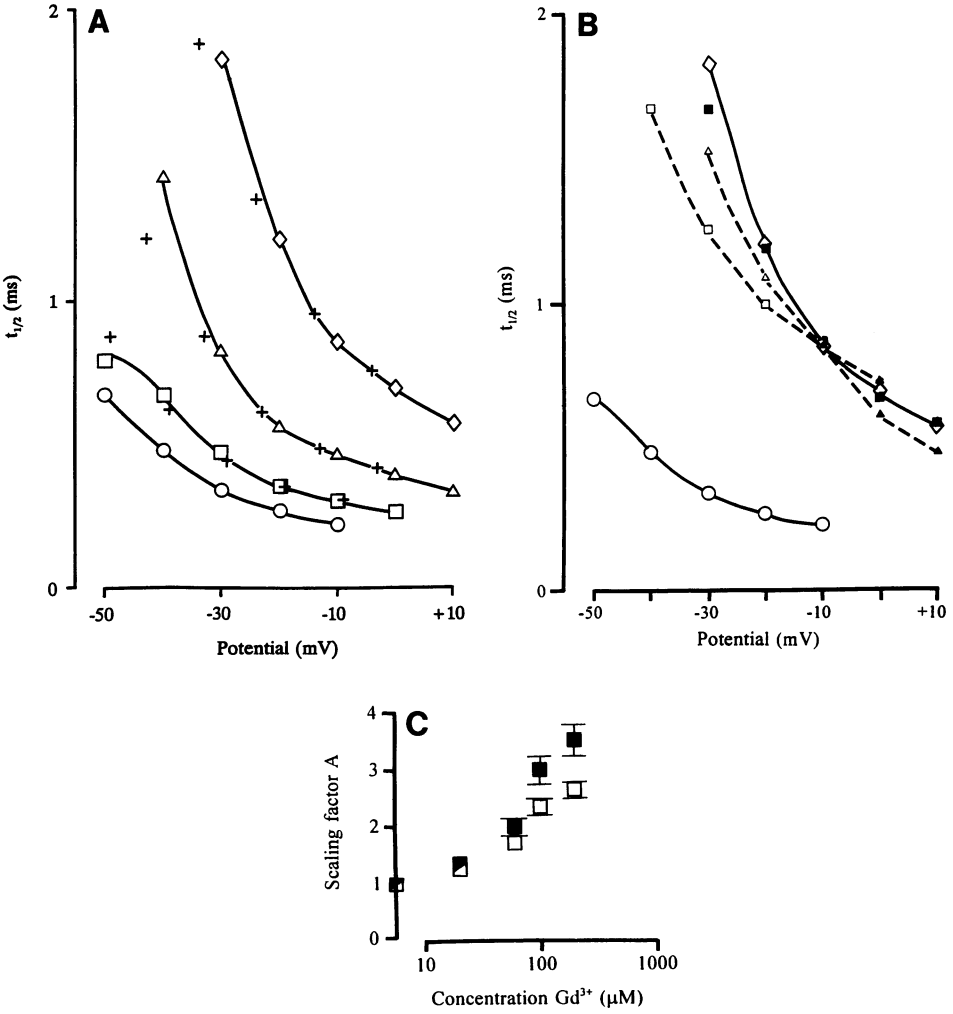

FIGURE 6 Effect on time course of I_{Na} activation. (*A*) Relation between $t_{1/2}$ and potential for control (○), 20 μM (□), 60 μM (△), and 200 μM Gd^{3+} (◇) solutions. U_H = −110 mV. Open symbols indicate experimental results from one fiber. Values calculated from control values on the assumption of a shift along the potential axis (ΔU_t) and scaling by a concentration-dependent factor (*A*) indicated by (+). For 20 μM, the values were ΔU_t = 1 mV and *A* = 1.3, for 60 μM ΔU_t = 7 mV and *A* = 1.8 and for 200 μM ΔU_t = 16 mV and *A* = 2.8. (*B*) Curves indicating validity of the shift-and-scaling procedure. Continuous lines from *A* for control (○) and for 200 μM Gd^{3+} (◇) solutions. Interrupted lines calculated for other combinations of shift and scaling values, chosen to give an intersection point at −10 mV: (□) ΔU_t = 0 mV, *A* = 3.7; (△) ΔU_t = 10 mV, *A* = 3.2; (■) ΔU_t = 20 mV, *A* = 2.5; (▲) ΔU_t = 30 mV, *A* = 1.8. (*C*) Dose-response curve for the scaling factor A. Values obtained directly from the shift-and-scaling procedure indicated by (□). Bars denote highest and lowest value obtained. Values corrected according to Fig. 12 to apply to effects on rate constants indicated by (■) (see Appendix). Values from two fibers.

a Gd^{3+}-induced modification of selectivity, as proposed to explain Ca^{2+} effects on K channels (Armstrong and Lopez-Barneo, 1987; Brismar and Collins, 1989; Armstrong and Miller, 1990).

Effect on K current

Shift of activation curve

As seen from Fig. 1, Gd^{3+} shifted the potential dependence of I_K in the positive direction. This is more evident in Fig. 9, which shows activation, calculated with Eq. 1 from measurements at 20, 40, and 80 ms. The effect could be described as a shift of the curve along the potential axis similar to the effect on the Na activation curve. As seen from the figure, the magnitude of the shift varied with time of measurement; the longer duration, the smaller the shift value. In the present investigation, the maximum pulse duration usually was 100 ms, thus avoiding interference by the inactivation, which became evident above 200 ms pulse durations. Rough approximations indicated that the Gd^{3+}-induced shift of the K activation curve reached a minimum after about 500 ms. For 60 μM Gd^{3+}, this minimum shift was about 10 mV (compared with 18 mV after 100 ms), which is close to the shift obtained for the Na system (see Fig. 4).

Activation-independent block

As indicated in Fig. 9, the fully activated I_K in Gd^{3+} solution showed a negligible potential dependence up to 60 mV. Above this point, the potential dependence was difficult to estimate because of the rectification of the I_K-*U* curve. To obtain a dose-response curve for this potential-independent block of I_K, we measured the current at the end of a 40-ms step to +50 mV from U_H of −90 mV. Fig. 2 *C* shows the dose response curve from measurements on seven fibers. K_d was 78 μM (*n* = 7; Table 1). K_H was 0.94 (*n* = 3; Table 1), suggesting 1:1 stoichiometry.

Effect on time course

Fig. 1 also shows that Gd^{3+} modifies the time course of the I_K activation. At a pulse step to +50 mV, 60 μM Gd^{3+} increased $t_{1/2}$ about 5 times and 200 μM about 7 times. The time constant curves for two concentrations are shown in Fig. 10 *A*. As in the case of the Na system, the effect could not be described as a simple shift along the potential axis (see *dashed line* in Fig. 10 *A*). The best fit was obtained by a combination of a shift (ΔU_t) and a multiplication by a concentration-dependent scaling factor (*A*). Unique value-pairs (ΔU_t/*A*) were obtained by a fitting procedure as shown

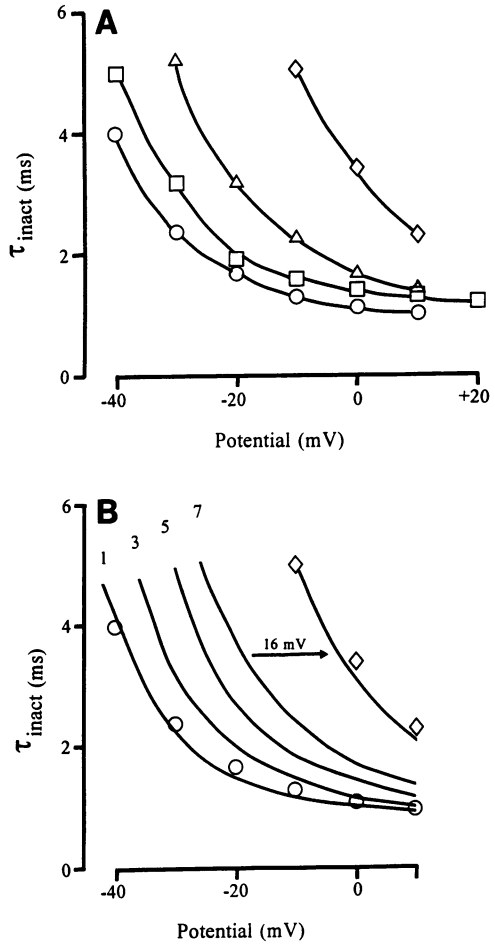

FIGURE 7 Effect on time course of I_{Na} inactivation. (*A*) Relation between time constants and potential for control (○), 20 μM (□), 60 μM (△), and 200 μM Gd^{3+} (◇) solutions. U_H = −110 mV. (*B*) Curves calculated from Model 1 in the Appendix for different scaling values (indicated) of the activation rate constants. Experimental points for control (○) and 200 μM Gd^{3+} (◇) solutions from *A*. Curve fitted to the 200 μM Gd^{3+} values was the curve for A = 7 shifted +16 mV. The curve fitted to control solution was computed on basis of the values in Frankenhaeuser and Huxley (1964) and with $B(\alpha_m)$ = 37 mV, and $C(\alpha_m)$ = 15 mV.

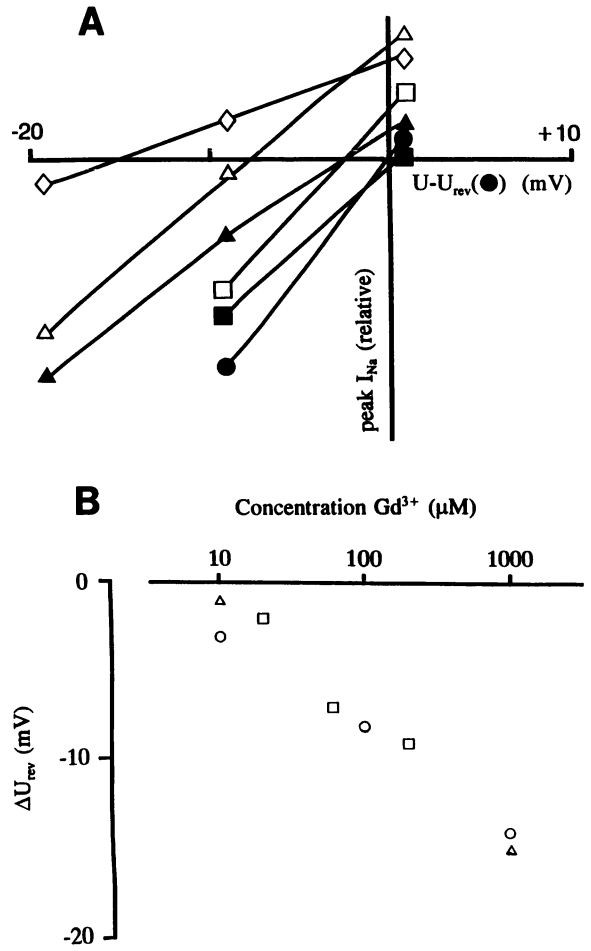

FIGURE 8 Effect on I_{Na} reversal potential (U_{rev}). (*A*) Peak I_{Na} versus relative potential, where U_{rev} in the first control solution is set to zero. Application in temporal order: Control (●), 10 μM (□), control (■), 100 μM (△), control (▲), and 1000 μM Gd^{3+} (◇) solutions. (*B*) Relation between shift of U_{rev} and concentration of Gd^{3+}. Data from three fibers as indicated by symbols.

for the Na system. The ΔU_t value obtained in this way for the highest concentration analyzed (200 μM) was +21 mV, and A was 5.7. Values of ΔU for four different concentrations are shown in Fig. 4 (△). They are well described by Eq. 1 for a surface charge density of −1.2 e nm^{-2}. Corresponding A values are plotted in Fig. 10 *B*.

DISCUSSION

The action of Gd^{3+} on the myelinated nerve fiber analyzed in the present investigation could be separated into the following main effects: (i) A positive shift of potential-dependent parameters of both Na and K channels was seen. The shifts were equally large for the activation, inactivation, and activation time constant curves, whereas it was larger for the inactivation time constant curve. (ii) A decrease of the rate of gating for both Na and K channels in addition to that caused by the shift (mentioned above) was seen. The effect was quantified as a potential-independent scaling of the activation time constant curves. (iii) An activation- and inactivation-independent block of Na and K channels was seen. (iv) A potential-independent block of I_L was seen.

A key finding was that the effect on time constant curves could be described as a unique combination of a shift and a scaling. This is in contrast to most other studies of metal ion effects on voltage-gated channels, which only report shifts. However, a dual effect has previously been noted for Ni^{2+} (Dodge, 1961), H^+ (Carbone et al., 1981), and for the intravenous general anesthetic propofol (Veintemilla et al., 1992), but no quantitative analysis has been performed.

In the following section, we will argue that the effects mentioned above under (i) to (iv) are mediated by separate mechanisms, with separate sites of action. We will also discuss possible binding sites for Gd^{3+}, with reference to available biochemical data. Aspects of the effect on I_L have been discussed elsewhere (Elinder and Århem, 1991b).

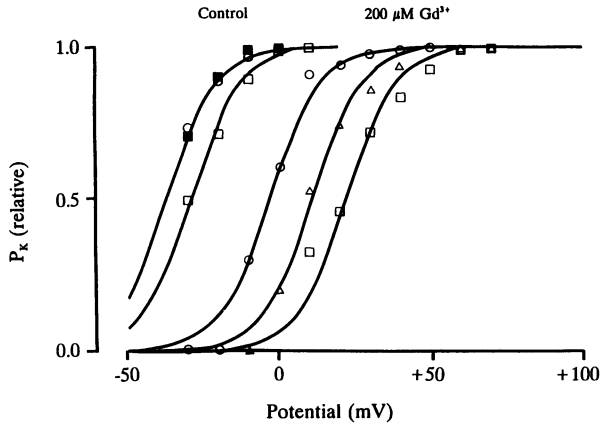

FIGURE 9 Shift of steady-state K activation curve. The two curves to the left apply to control solution before (*closed symbols*) and after (*open symbols*) application of test solution. The three curves to the right apply to 200 μM Gd^{3+} solution. Measurements after 20 ms (□), 40 ms (△), and 80 ms (○). Continuous lines solutions to Eq. 2 for $U_{1/2}$ = −37 mV, −29 mV, −3 mV, +11 mV and +22 mV. k = 9.0 mV.

Mechanism of voltage-dependent parameter shifts

The shifts of the activation and time constant curves obtained after our separation between shift and scaling effects were found to be perfectly compatible with a surface charge hypothesis. As seen from Fig. 4, the shift values obtained well fit the Grahame equation (Eq. 3) for a charge density of −1.2 e nm^{-2} for both Na and K channels. The finding that at first might seem difficult to explain within this explanation is the large shift of the inactivation time constant curve compared with that of the corresponding activation curve (Fig. 7 *A*). However, taking the scaling effect into account, as will be discussed in the next section, the finding is fully compatible with the proposed explanation.

As mentioned in the Introduction, the surface charge hypothesis has many shortcomings, the most serious being that parameters of one gating function are reported to be unequally shifted (Hille, 1992). Armstrong and Cota (1990) have even reported that La^{3+} shifted Na channel deactivation and activation time (rate) constant curves in opposite directions, thereby excluding any modification of a surface charge hypothesis as explanation. However, by using our separation procedure, it is possible to explain their data within a surface charge hypothesis. Fig. 11 shows their data for La^{3+} effects on Na channel activation and deactivation rate constants. Inspection of the figure shows that the effect cannot be described as a pure shift. However, it can be described as a combined shift and scaling. For 10 μM La^{3+}, the best fit for the shift of the deactivation rate constant curve was between 0 and 5 mV, and for the activation rate constant curve, it was between 5 and 10 mV. The corresponding scaling values were between 1.2 and 1.6 (given as reciprocal value of the factor describing the reduction of the rate constant). For 2 mM La^{3+}, the shift values were between 35 and 45 mV, and the scaling values were between 1.4 and 2.0 (both activation and deactivation values included). Thus, shift and scaling values were approximately equal for the activation and the deactivation rate constant curves at a certain concentration. Assuming equal shift and scaling values for activation and deactivation rate constant curves, the best fits obtained were ΔU_t = 5 mV and A = 1.6 for 10 μM La^{3+} and ΔU_t = 39 mV and A = 1.8 for 2 mM (Fig. 11), suggesting a surface charge density of −1.4 e nm^{-2}. The shift values obtained are in good agreement with the values for the activation curve (+2.2 and +42.5 mV). In a similar way, it was possible by a separation

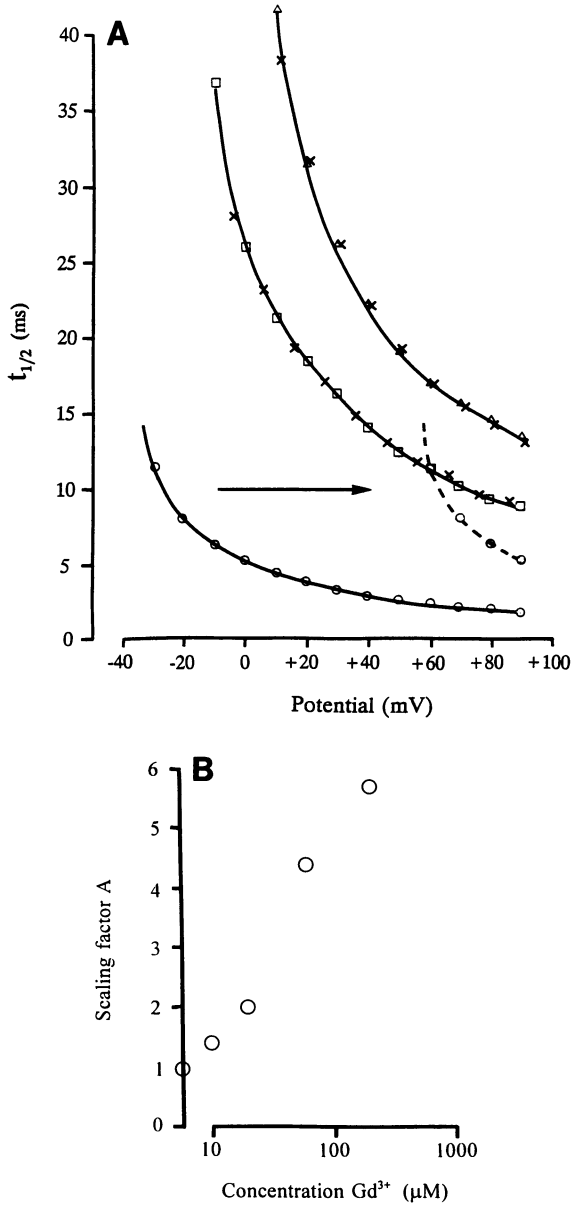

FIGURE 10 Effect on time course of I_K activation. (*A*) Relation between $t_{1/2}$ and potential for control (○), 60 μM (□) and 200 μM Gd^{3+} (△) solutions. Open symbols indicate experimental results from one fiber. Values calculated from control values on the assumption of a shift (ΔU_t) and a scaling (A) indicated by (x). For 60 μM, the values were ΔU_t = 6 mV and A = 4.4 and for 200 μM ΔU_t = 21 mV and A = 5.7. Interrupted line and arrow show the case of exclusively a shift (+90 mV). (*B*) Dose-response curve for the scaling factor A. Values from two fibers.

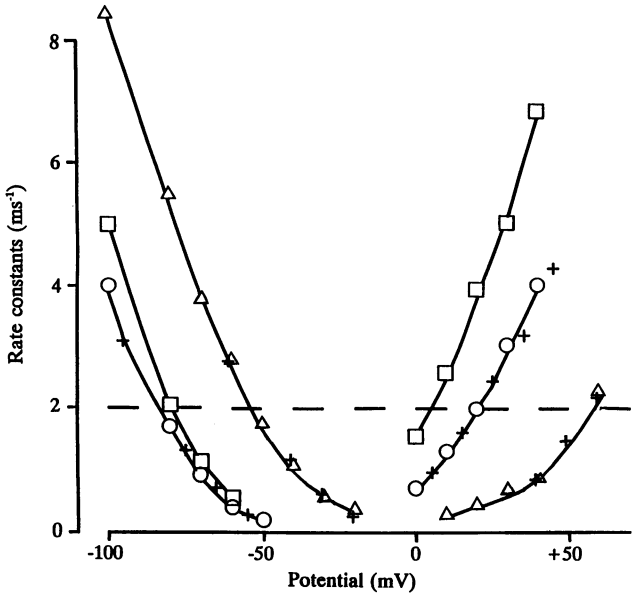

FIGURE 11 Effects of La^{3+} on Na channel rate constants from GH3 cells. Open symbols denote experimental data from Armstrong and Cota (1990). Solutions contained 2 mM Ca^{2+} (□), 10 μM La^{3+} (○), and 2 mM La^{3+} (△), respectively. Left panel shows deactivation constants, and right panel shows activation constants. Values calculated from values in the 2 mM Ca^{2+} solution on the assumption of a shift and a scaling ($1/A$) equal for activation and deactivation indicated by (+). For 10 μM La^{3+} the values were ΔU_t = 5 mV and A = 1.6 and for 2 mM La^{3+} ΔU_t = 39 mV and A = 1.8. The interrupted line indicates the level at which Armstrong and Cota measured the shift.

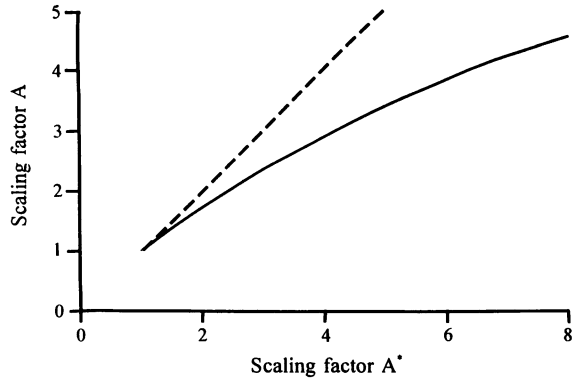

FIGURE 12 The relation between the measured scaling factor A and the corrected scaling factor A* applying to rate constants (——). The dashed line is $A = A^*$.

procedure to account for reported differences in shifts of activation and deactivation time constant curves induced by the group IIA and IIB ions Ba^{2+}, Zn^{2+}, Cd^{2+}, and Hg^{2+} (Gilly and Armstrong, 1982a, b; Cukierman and Krueger, 1990, 1991; Agus et al., 1991).

The surface charge density obtained for the nodal Na and K channels in the present investigation was −1.2 e nm^{-2}, calculated on the assumption of exclusive screening and no binding (the Gouy-Chapman theory). This value is in agreement with estimations from other studies. The geometric means of the values collected by Gilbert and Ehrenstein (1984) for axonal Na and K channels were for frog −0.6 and −0.4 e nm^{-2}, for squid −1.1 and −0.9 e nm^{-2}, and for Myxicola −1.0 and −0.6 e nm^{-2}.

Mechanism of time constant scaling

The Gd^{3+}-induced scaling of time constant curves in addition to the induced shift along the potential axis, suggest Gd^{3+} binding to an extracellular modulatory site on the channel (both Na and K channels). A quantitative model for the time constant effects in terms of effects on activation and deactivation rate constants was developed as described in the Appendix. It assumes that the reduction of the activation and deactivation rate constants is equally large (see discussion of the Armstrong and Cota findings above). The description of the channel kinetics used was that developed on basis of the experimental results of Elinder and Århem (1991a). The model implies that the experimentally found A values for the time constant scaling of the K channel can be directly used to describe the reduction of the rate constants (by the factor A), whereas the relation between the corresponding values of the Na system is more complicated. For further quantitative treatment in the subsequent paper (Elinder and Århem, 1994), therefore, we computed the relation between scaling value of the time constant (A) and the reciprocal scaling value of activation and deactivation rate constants (A^*) for the Na channel (Fig. 12).

The presented scaling effect model can be used to compute the effects of Gd^{3+} on the inactivation. Fig. 7 *B* shows inactivation time constant curves computed for different scaling effects on the activation rate constants. From the figure, it is clear that for any chosen A^* value, a ΔU value can be chosen to explain the effect. Assuming the shift being between 16 and 23 mV (see Fig. 4), the corresponding scaling factor is between 5 and 7, in relative agreement with the observed data (Fig. 6 *B*). We conclude that the effect on the inactivation time constant cannot be used to refute a surface charge hypothesis.

The scaling effect model can also be used to explain the specific slope reduction of the Na activation curve at high Gd^{3+} concentrations (Fig. 3 *C*). Computations showed that A^* = 3.5, corresponding to the effect of 200 μM Gd^{3+}, decreases the slope by 17%, close to the observed value. The reduction depends principally on the assumption in the model that the Gd^{3+} binding exclusively affects the activation and deactivation rate constants, the corresponding inactivation rate constants being unaffected. The importance of the inactivation system in this context seems to be in accordance with experimental findings; Ba^{2+} is reported not to reduce the slope in batrachotoxin-treated Na channels, where the inactivation is removed (Cukierman and Krueger, 1990, 1991), whereas it reduces the slope when inactivation is intact (Brismar, 1980; Hanck and Sheets, 1992). Corresponding computations on the K channel showed no slope reduction, in accordance with the experimental results. However, it should be mentioned here that Armstrong and Cota (1990)

have reported an La^{3+}-induced slope reduction of the Na activation curve in papain-treated GH3 cells where the inactivation was absent. This will be treated in the subsequent paper (Elinder and Århem, 1994).

As mentioned above, a scaling effect has not been explicitly shown for other metal ions. However, such an effect can be inferred from other studies. The group IIB elements Zn^{2+}, Cd^{2+}, and Hg^{2+} and the transition elements Cu^{2+} and Ni^{2+} as well as the trivalent La^{3+} seem to have scaling factors larger than 1.5, whereas those of the group IIA elements Mg^{2+}, Ca^{2+}, and Ba^{2+} and the transition elements Mn^{2+} and Co^{2+} are smaller at equipotent concentrations (Århem, 1980b; Gilly and Armstrong, 1982b; Armstrong and Cota, 1990; Cukierman and Krueger, 1990, 1991; Agus et al., 1991; Fan and Hiraoka, 1991).

In summary, the presented explanation for the effects of Gd^{3+} and other metal ions on potential-dependent parameters, assuming both screening and scaling mediated by an extracellular modulatory site, seems to account for most of the presented findings as well as for findings reported in the literature. This explanation should be seen in relation to other attempts to explain the total action of metal ions, including effects other than screening. At least two such detailed attempts have been made. (1) Armstrong and co-workers (Gilly and Armstrong, 1982a, b; Armstrong and Cota, 1990, 1991) have proposed a model without invoking screening at all, assuming an extracellular modulatory site associated with the opening of the channels but not with the closing. A difficulty with this model is that it does not explain their own finding of an La^{3+}-induced acceleration of Na channel closing (Armstrong and Cota, 1990; and Fig. 11 for 2 mM). (2) Cukierman and Krueger (1990, 1991) have proposed a similar model, but one that includes screening and both extra and intracellular modulatory sites, the extracellular site being associated with opening of channels and the intracellular with closing. A difficulty with this model is that it neither explains the decreased rate of Na channel closing, induced by externally applied La^{3+} (Armstrong and Cota, 1990; Fig. 11 for 10 μM), nor the decreased rate of opening, induced by internally applied Zn^{2+} (Fox et al., 1974). As already indicated, assuming a unitary metal ion action on the activation/deactivation rate constants rather than a selective, as proposed in the present investigation, avoids the difficulties encountered by the attempts mentioned above.

Mechanism of block

The observed activation- and inactivation-independent reduction of the currents is most simply explained by a reduced number of channels, caused by a direct block. Such a block seems to be the main cause of the I_K reduction, whereas at least two further mechanisms are predicted to contribute considerably to the I_{Na} reduction. (i) Screening will reduce the Na concentration at the surface of the membrane, thereby reducing the channel conductance, as has been reported for the action of externally applied La^{3+}, Ni^{2+}, and H^+ on axonal Na channels (Conti et al., 1976; Sigworth, 1980; Neumcke and Stämpfli, 1984). (ii) Differential scaling of activation and inactivation rate constants, as assumed in our model, will reduce the peak permeability. At 100 μM Gd^{3+} (Fig. 4), the screening effect is calculated to decrease the surface Na concentration by 31% (assuming ΔU = 9 mV and the relative surface concentration equal to $\exp(-\Delta UF/RT)$), and the scaling effect is calculated to decrease the peak permeability by 20% (computations based on the model in Appendix and assuming A^* = 3), suggesting a direct block effect of about 30%.

In conclusion, a considerable fraction of the activation- and inactivation-independent reduction of I_{Na} and I_K can be assumed to be caused by a direct block of channels, mediated by a blocking site separate from the modulatory site. Such a block has been proposed for several divalent metal ions and for La^{3+} (Armstrong and Cota, 1990, 1991; Sheets and Hanck, 1992). The weak potential dependence of the K channel block indicates that the blocking site is located close to the external surface. This is in accordance with reported Na channel block of La^{3+} and the group IIB elements Cd^{2+} and Zn^{2+}, whereas it seems to differ from the clearly potential-dependent block of the group IIA elements Mg^{2+}, Ca^{2+}, and Ba^{2+}, and the transition elements Co^{2+} and Mn^{2+}, whose site of binding has been proposed to be located one-third of the way into the membrane electric field (Sheets and Hanck, 1992).

Binding sites

From above, it is clear that the concentration dependence varied for the different effects. The reduction of I_L, I_{Na}, and I_K and the increase of the time constants could be described by equations for a reversible binding reaction with different stoichiometry and different K_d values. The effect on I_L showed 1:2 stoichiometry and had a relatively high K_d value (about 600 μM); the effect on I_{Na} and I_K showed 1:1 stoichiometry with relatively low K_d values (70 to 80 μM), and the time constant effect also had relatively low K_d values (approximately 30 to 100 μM).

Lanthanides (Ln^{3+}) have been reported to bind to two classes of sites on biomembranes; less abundant high affinity sites with K_d values in the 0.5–50 μM range and low affinity sites in the 10–1000 μM range (for a review, see Evans, 1990). Proteins have been shown to bind Ln^{3+} strongly, and phospholipids less strongly. It has been suggested that La^{3+} binds to Ca channels in neuroblastoma cells (El-Fakahany et al., 1983). The stoichiometry of the Ln^{3+} binding seems to differ for the low and high affinity sites. 1:2 complexes between Ln^{3+} and charged phosphate groups in phosphatidylcholine in membranes have been reported (Hauser et al., 1976).

The present findings could be reconciled with the biochemical results by assuming that Gd^{3+} binds to high affinity sites on Na and K channel proteins with 1:1 stoichiometry and to low affinity sites, related to I_L, on phospholipids with 1:2 stoichiometry. This suggests that I_L is caused by passage of ions through protein-independent but phospholipid-

dependent pathways. On the other hand, other studies suggest that channel proteins are necessary for I_L (Armstrong and Miller, 1990). To explain these conflicting findings, we have tentatively proposed a leakage pathway at the interface between channel proteins and the lipid phase (Elinder and Århem, 1991b).

CONCLUSIONS

In conclusion, the findings suggest at least four types of mechanism, and four sites of action, for the action of Gd^{3+} on myelinated nerve fibers: (i) A reduction of I_L by relatively low affinity binding to phospholipids by 1:2 stoichiometry. (ii) A modification of the electric field over the membrane by neutralizing uniform fixed surface charges at a density of -1.2 e nm^{-2} (the Gouy-Chapman theory) or lower (the Gouy-Chapman-Stern theory), causing a shift of potential-dependent parameters along the potential axis. (iii) An additional slowing of the time course of I_{Na} and I_K by high affinity binding to modulatory sites on the channels. (iv) A reduction of I_{Na} and I_K by high affinity binding to blocking sites on the channels with 1:1 stoichiometry. The discussed comparison with other studies in the literature further suggests that the effects by other metal ions are mediated by the same sites. Ca^{2+} especially, physiologically the most abundant polyvalent cation, is expected to have similar effects, because of its close chemical relation to Gd^{3+} (see Introduction).

A general conclusion should finally be mentioned. Gd^{3+} should be used with caution to separate stretch-activated channels from voltage-gated channels, because the effective concentration range was the same as that reported to induce effects on some types of such channels (Yang and Sachs, 1989; Swerup et al., 1991; Zhou et al., 1991).

We thank Dr. Bo Rydqvist, Department for Physiology II at Karolinska Institutet, for providing the gadolinium chloride and Dr. Russell Hill, Department of Neuroscience at Karolinska Institutet, for valuable comments on the manuscript.

This work was supported by grants from the Swedish Medical Research Council (project No 6552), The Karolinska Institute, and the Swedish Society for Medical Research.

APPENDIX

A quantitative model for the scaling effect

This section describes the quantitative model for the scaling effect on activation and inactivation time constant curves, used for the computations in the text. The model assumes channel kinetics according to the equations developed by Elinder and Århem (1991a) to acount for the currents in the amphibian node of Ranvier. The scaling of the time constants, described by factor A, was assumed to be mediated by a scaling of activation and deactivation rate constants, described by the reciprocal value of factor A^*. This factor was assumed to be equal for activation and deactivation rate constants. Further, the inactivation rate constants were assumed to be unaffected. Using this model, it is possible to compute (a) the relation between the observed scaling factor A and the postulated A^* factor (for the rate constants), (b) the effect of scaling on the slope of the Na channel activation curve, and (c) the effect of scaling on the inactivation time constant curve.

The kinetics of the Na channel assumes a strict coupling between activation and inactivation (see Bezanilla and Armstrong, 1977; Gilly and Armstrong, 1982a) as described by the following state diagram:

$$\mathrm{C1} \underset{1.4\beta_m}{\overset{1.4\alpha_m}{\rightleftharpoons}} \mathrm{C2} \underset{1.4\beta_m}{\overset{1.4\alpha_m}{\rightleftharpoons}} \mathrm{O} \underset{0.002\ \mathrm{ms}^{-1}}{\overset{1.0\ \mathrm{ms}^{-1}}{\rightleftharpoons}} \mathrm{I} \qquad \text{(Model 1)}$$

C1 and C2 denote closed states, O an open state, and I an inactivated state. α_m and β_m are determined by Eqs. 13 and 14 in Frankenhaeuser and Huxley (1964), and are temperature-corrected (Frankenhaeuser and Moore, 1963). The scaling was obtained by dividing rate constants α_m and β_m with the factor A^*. The computational procedure was essentially performed as described in Elinder and Århem (1991a).

The relation between A^* and A was determined by computation of the time course of the open state for different A^* values at different potentials and subsequent estimation of corresponding A values. The relation showed almost no voltage dependence and is shown in Fig 12. Computations further showed that an A^* value of 3.5 (corresponding to the effect of 200 μM Gd^{3+}) shifted the activation curve 4 mV in the positive direction along the potential axis and that the slope of the same curve was decreased with 17%, in accordance with the experimental results (Fig. 3 *B*). Computations of the inactivation time constant curve for different A^* values is shown in Fig. 7 *B*.

The kinetics of the K channel was described by the following state diagram:

$$\mathrm{C1} \underset{1.4\beta_n}{\overset{1.4\alpha_n}{\rightleftharpoons}} \mathrm{C2} \underset{1.4\beta_n}{\overset{1.4\alpha_n}{\rightleftharpoons}} \mathrm{O} \qquad \text{(Model 2)}$$

C1 and C2 denote closed states, O denotes an open state, and α_n and β_n are determined by Eqs. 13 and 14 in Frankenhaeuser and Huxley (1964), and are temperature-corrected (Frankenhaeuser and Moore, 1963). The scaling was obtained by dividing rate constants α_n and β_n with a factor A^*. In this case, the scaling factor for the activation time constant A equals A^*. Computations showed that an A^* value of 5.7 (corresponding to 200 μM Gd^{3+}) did not measurably modify the activation curve, in accordance with the experimental results (Fig. 9).

REFERENCES

Adelman, W. J., and R. E. Taylor. 1961. Leakage current rectification in the squid giant axon. *Nature.* 190:883–885.

Agus, Z. S., I. D. Dukes, and M. Morad. 1991. Divalent cations modulate the transient outward current in rat ventricular myocytes. *Am. J. Physiol.* 261:C310–C318.

Århem, P. 1980a. Effects of rubidium, caesium, strontium, barium and lanthanum on ionic current in myelinated nerve fibres from *Xenopus laevis*. *Acta Physiol. Scand.* 108:7–16.

Århem, P. 1980b. Effects of some heavy metal ions on the ionic currents of myelinated fibres from *Xenopus laevis*. *J. Physiol.* 306:219–231.

Århem, P., B. Frankenhaeuser, and L. E. Moore. 1973. Ionic currents at resting potential in nerve fibres from *Xenopus laevis*. Potential clamp experiments. *Acta Physiol. Scand.* 88:446–454.

Armstrong, C. M., and G. Cota. 1990. Modification of sodium channel gating by lanthanum. *J. Gen. Physiol.* 96:1129–1140.

Armstrong, C. M., and G. Cota. 1991. Calcium ion as a cofactor in Na channel gating. *Proc. Natl. Acad. Sci. USA.* 88:6528–6531.

Armstrong, C. M., and J. Lopez-Barneo. 1987. External calcium ions are required for potassium channel gating in squid neurons. *Science.* 236: 712–714.

Armstrong, C. M., and C. Miller. 1990. Do voltage-dependent K^+ channels require Ca^{2+}? A critical test employing a heterologous expression system. *Proc. Natl. Acad. Sci. USA.* 87:7579–7582.

Bezanilla, F., and C. M. Armstrong. 1977. Inactivation of the sodium channel. I. Sodium current experiments. *J. Gen. Physiol.* 70:549–566.

Biedermann, G., and L. Ciavatta. 1961. Studies on the hydrolysis of metal ions. Part 35. The hydrolysis of the lanthanum ion, La^{3+}. *Acta Chem. Scand.* 15:1347–1366.

Brismar, T. 1973. Effects of ionic concentration on permeability properties of nodal membrane in myelinated nerve fibres of *Xenopus laevis*. Potential clamp experiments. *Acta Physiol. Scand.* 87:474–484.

Brismar, T. 1980. The effect of divalent and trivalent cations on the sodium permeability of myelinated nerve fibres of *Xenopus laevis*. *Acta Physiol. Scand.* 108:23–29.

Brismar, T., and V. P. Collins. 1989. Potassium and sodium channels in human malignant glioma cells. *Brain Res.* 480:259–267.

Carbone, E., P. L. Testa, and E. Wanke. 1981. Intracellular pH and ionic channels in the *Loligi vulgaris* giant axon. *Biophys. J.* 35:393–413.

Chandler, W. K., A. L. Hodgkin, and H. Meves. 1965. The effect of changing the internal solution on sodium inactivation and related phenomena in giant axons. *J. Physiol.* 180:821–836.

Conti, F., B. Hille, B. Neumcke, W. Nonner, and R. Stämpfli. 1976. Measurement of the conductance of the sodium channel from current fluctuations at the node of Ranvier. *J. Physiol.* 262:699–727.

Cukierman, S., and B. K. Krueger. 1990. Modulation of sodium channel gating by external divalent cations: differential effects on opening and closing rates. *Pflügers Arch.* 416:360–367.

Cukierman, S., and B. K. Krueger. 1991. Effects of internal divalent cations on the gating of rat brain Na^+ channels reconstituted in planar lipid bilayers. *Pflügers Arch.* 419:559–565.

Docherty, R. J. 1988. Gadolinium selectively blocks a component of calcium current in rodent neuroblastoma x glioma hybrid (NG108–15) cells. *J. Physiol.* 398:33–47.

Dodge, F. A. 1961. Ionic permeability changes underlying nerve excitation. *In* Biophysics of Physiological and Pharmacological Actions. American Association for the Advancement of Science, Washington, D. C. 119–143.

Dodge, F. A., and B. Frankenhaeuser. 1958. Membrane currents in isolated frog nerve fibre under voltage clamp conditions. *J. Physiol.* 143: 76–90.

Dodge, F. A., and B. Frankenhaeuser. 1959. Sodium currents in the myelinated nerve fibre of *Xenopus laevis* investigated with the voltage clamp technique. *J. Physiol.* 148:188–200.

Dubois, J. M. 1981. Evidence for the existence of three types of potassium channels in the frog ranvier node membrane. *J. Physiol.* 318:297–316.

Dubois, J. M., and C. Bergman. 1971. Conductance sodium de la membrane nodale: inhibition compétitive calcium-sodium. *C. R. Acad. Sci. III* 272: 2924–2927.

El-Fakahany, E., J. R. Lopez, and E. Richelson. 1983. Lanthanum binding to murine neuroblastoma cells. *J. Neurochem.* 40:1687–1691.

Elinder, F., and P. Århem. 1991a. Mechanisms of the tetrahydroaminoacridine effect on action potential and ion currents in myelinated axons. *Eur. J. Pharmacol.* 208:1–8.

Elinder, F., and P. Århem. 1991b. Properties of the leakage current pathway: effects of the gadolinium ion on myelinated axon. *NeuroReport.* 2: 685–687.

Elinder, F., and P. Århem. 1994. A modulatory site for the action of gadolinium on surface charges and channel gating. *Biophys. J.* 67: 84–90.

Evans, C. H. 1990. Biochemistry of the Lanthanides. Plenum Press, New York. 444 pp.

Fan, Z., and M. Hiraoka. 1991. Depression of delayed outward K^+ current by Co^{2+} in guinea pig ventricular myocytes. *Am. J. Physiol.* C23–C31.

Fox, J. M., E. Rojas, and R. Stämpfli. 1974. Blocking of sodium and potassium conductance by internal application of Zn^{++} in the node of Ranvier. *Pflügers Arch.* 351:271–274.

Frankenhaeuser, B. 1962. Potassium permeability in myelinated nerve fibres of *Xenopus laevis*. *J. Physiol.* 160:54–61.

Frankenhaeuser, B., and A. L. Hodgkin. 1957. The action of calcium on the electrical properties of squid axons. *J. Physiol.* 137:218–244.

Frankenhaeuser, B., and A. F. Huxley. 1964. The action potential in the myelinated nerve fibre of *Xenopus laevis* as computed on the basis of voltage clamp data. *J. Physiol.* 171:302–315.

Frankenhaeuser, B., and L. E. Moore. 1963. The effect of temperature on the sodium and potassium permeability changes in myelinated nerve fibres of *Xenopus laevis*. *J. Physiol.* 169:431–437.

Frausto da Silva, J. J. R., and R. J. P. Williams. 1991. The Biological Chemistry of the Elements. Clarendon Press, Oxford. 561 pp.

Gilbert, D. L., and G. Ehrenstein. 1969. Effect of divalent cations on potassium conductance of squid axons: determination of surface charge. *Biophys. J.* 9:447–463.

Gilbert, D. L., and G. Ehrenstein. 1984. Membrane surface charge. *Curr. Topics Membr. Transp.* 22:407–421.

Gilly, W. F., and C. M. Armstrong. 1982a. Slowing of sodium channel opening kinetics in squid axon by extracellular zinc. *J. Gen. Physiol.* 79:935–964.

Gilly, W. F., and C. M. Armstrong. 1982b. Divalent cations and the activation kinetics of potassium channels in squid giant axons. *J. Gen. Physiol.* 79:965–996.

Goldman, D. E. 1943. Potential, impedance, and rectification in membranes. *J. Gen Physiol.* 27:37–60.

Grahame, D. C. 1947. The electrical double layer and the theory of electrocapillarity. *Chem. Rev.* 41:441–501.

Hanck, D. A., and M. F. Sheets. 1992. Extracellular divalent and trivalent cation effects on sodium current kinetics in single canine cardiac purkinje cells. *J. Physiol.* 454:267–298.

Hauser, H., M. C. Phillips, B. A. Levine, and R. J. P. Williams. 1976. Conformation of the lecithin polar group in charged vesicles. *Nature.* 261:390–394.

Hille, B. 1992. Ionic Channels of Excitable Membranes. Sinauer, Sunderland, MA. 612 pp.

Hille, B., A. M. Woodhull, and B. I. Shapiro. 1975. Negative surface charge near sodium channels of nerve: divalent ions, Monovalent ions, and pH. *Phil. Trans. R. Soc. Lond. B.* 270:301–318.

Hodgkin, A. L., and B. Katz. 1949. The effect of sodium ions on electrical activity of the giant axon of the squid. *J. Physiol.* 108:37–77.

Huxley, A. F., and R. Stämpfli. 1951. Direct determination of membrane resting potential and action potential in single myelinated nerve fibres. *J. Physiol.* 112:476–495.

Lansman, J. B. 1990. Blockade of current through single calcium channels by trivalent lanthanide cations. Effect of ionic radius on the rates of ion entry and exit. *J. Gen Physiol.* 95:679–696.

McLaughlin, S. 1989. The electrostatic properties of membranes. *Annu. Rev. Biophys. Biophys. Chem.* 18:113–136.

Neumcke, B., and R. Stämpfli. 1984. Heterogeneity of external surface charges near sodium channels in the nodal membrane of frog nerve. *Pflügers Arch.* 401:125–131.

Rack, M., and G. Drews. 1989. Effects of a synthetic cationic polymer on sodium and potassium currents of frog nerve fibres. *Pflügers Arch.* 413: 610–615.

Sheets, M. F., and D. A. Hanck. 1992. Mechanisms of extracellular divalent and trivalent cation block of the sodium current in canine cardiac purkinje cells. *J. Physiol.* 454:299–320.

Sigworth, F. J. 1980. The conductance of sodium channels under conditions of reduced current at the node of Ranvier. *J. Physiol.* 307:131–142.

Smith, R. M., and A. E. Martell. 1976. Critical Stability Constants. Vol. 4. Inorganic Complexes. Plenum Press, New York. 263 pp.

Swerup, C., N. Purali, and B. Rydqvist. 1991. Block of receptor response in the stretch receptor neuron of the crayfish by gadolinium. *Acta Physiol. Scand.* 143:21–26.

Veintemilla, F., F. Elinder, and P. Århem. 1992. Mechanisms of propofol action on ion currents in the myelinated axon of *Xenopus laevis*. *Eur. J. Pharmacol.* 218:59–68.

Takata, M., W. F. Pickard, J. Y. Lettvin, and J. W. Moore. 1966. Ionic conductance changes in lobster axon membranes when lanthanum is substituted for calcium. *J. Gen Physiol.* 50:461–472.

Vogel, W. 1974. Calcium and lanthanum effects at the nodal membrane. *Pflügers Arch.* 350:25–39.

Yang, X.-C., and F. Sachs. 1989. Block of stretch-activated ion channels in Xenopus oocytes by gadolinium and calcium ions. *Science.* 243: 1068–1071.

Zhou, X.-L., M. A. Stumpf, H. C. Hoch, and C. Kung. 1991. A mechanosensitive channel in whole cells and in membrane patches of the fungus Uromyces. *Science.* 253:1415–1417.